

ARMY RESEARCH LABORATORY



# Preliminary Electromagnetic Field Measurements Near an Electromagnetic Armor Experiment

by William O. Coburn, Calvin Le,  
and Brian Luu

ARL-MR-310

July 1996

19960725 052

Approved for public release; distribution unlimited.

DTIC QUALITY INSPECTED 1

The findings in this report are not to be construed as an official Department of the Army position unless so designated by other authorized documents.

Citation of manufacturer's or trade names does not constitute an official endorsement or approval of the use thereof.

Destroy this report when it is no longer needed. Do not return it to the originator.

<b>REPORT DOCUMENTATION PAGE</b>			Form Approved OMB No. 0704-0188	
Public reporting burden for this collection of information is estimated to average 1 hour per response, including the time for reviewing instructions, searching existing data sources, gathering and maintaining the data needed, and completing and reviewing the collection of information. Send comments regarding this burden estimate or any other aspect of this collection of information, including suggestions for reducing this burden, to Washington Headquarters Services, Directorate for Information Operations and Reports, 1215 Jefferson Davis Highway, Suite 1204, Arlington, VA 22202-4302, and to the Office of Management and Budget, Paperwork Reduction Project (0704-0188), Washington, DC 20503.				
1. AGENCY USE ONLY (Leave blank)		2. REPORT DATE July 1996		3. REPORT TYPE AND DATES COVERED Final, from 1 June 1994 to 1 July 1994
4. TITLE AND SUBTITLE Preliminary Electromagnetic Field Measurements Near an Electromagnetic Armor Experiment			5. FUNDING NUMBERS PE: 62120	
6. AUTHOR(S) William O. Coburn, Calvin Le, and Brian Luu				
7. PERFORMING ORGANIZATION NAME(S) AND ADDRESS(ES) U.S. Army Research Laboratory Attn: AMSRL-WT-ND 2800 Powder Mill Road Adelphi, MD 20783-1197			8. PERFORMING ORGANIZATION REPORT NUMBER ARL-MR-310	
9. SPONSORING/MONITORING AGENCY NAME(S) AND ADDRESS(ES) U.S. Army Research Laboratory 2800 Powder Mill Road Adelphi, MD 20783-1197			10. SPONSORING/MONITORING AGENCY REPORT NUMBER	
11. SUPPLEMENTARY NOTES AMS code: 622120.H250011 ARL PR: 5FE7E5				
12a. DISTRIBUTION/AVAILABILITY STATEMENT Approved for public release; distribution unlimited.			12b. DISTRIBUTION CODE	
13. ABSTRACT (Maximum 200 words)  We took a limited number of electric and magnetic field measurements near an electromagnetic (EM) armor experiment. The EM armor system forms a current channel that interferes with armor penetration between two electrified plates. We designed the field measurements to investigate the transient EM environment associated with the discharge of a capacitor bank through the electrified plates. We normalized the data to the measured peak current amplitude and the plate separation, and compared them to a model of the experimental configuration in terms of the source current elements. We considered an electrically small, transient source current filament over a perfect ground plane, where the EM field was calculated directly in the time domain. We estimated the effects of the plates on the EM field separately, based on the fringing field of a parallel plate capacitor in two dimensions. The combination of these simple models provides a useful engineering tool to predict the temporal and spatial variations of the EM environment associated with an EM armor system.				
14. SUBJECT TERMS Electromagnetic armor, EM environment, Walker-plate E-field, H-field			15. NUMBER OF PAGES 22	
			16. PRICE CODE	
17. SECURITY CLASSIFICATION OF REPORT Unclassified	18. SECURITY CLASSIFICATION OF THIS PAGE Unclassified	19. SECURITY CLASSIFICATION OF ABSTRACT Unclassified	20. LIMITATION OF ABSTRACT UL	

## Foreword

The Weapons Technology Directorate (WTD) of the Army Research Laboratory (ARL) has formulated a research program to investigate the electromagnetic (EM) environment produced by emerging technologies such as EM launch systems. This cooperative research program involves members of the Nuclear and Directed Energy (WT-ND), Weapons Concepts (WT-WD), Terminal Effects (WT-TA), and Propulsion and Flight (WT-PB) divisions. One advanced weapon concept of interest is EM armor, which uses a large current to disrupt a threat. This report describes the preliminary efforts in measuring the EM environment in the vicinity of electrified plate experiments. These experiments were conducted by the WT-WD and WT-TA divisions and provided an opportunity to measure the electric and magnetic fields that might be associated with an EM armor system. The results contribute to the technology base required to address the EM environment effects of advanced armor concepts.

## Contents

Foreword .....	iii
1. Introduction .....	1
2. Experiment .....	1
3. Analysis .....	3
3.1 EM Field of an Alternating Electric Current Element .....	4
3.2 Electrostatic Field of Semi-Infinite Plates .....	5
4. Results .....	7
4.1 EM Field Measurements for a Calibration Configuration .....	7
4.2 EM Field Measurements for a Live Munition Configuration .....	8
5. Conclusion .....	13
Acknowledgments .....	13
References .....	14
Distribution .....	15

## Figures

1. Field mapping coordinate system and Walker plate geometry imaged in a perfectly conducting ground plane .....	1
2. Analytical fit to normalized input current for live-fire and calibration conditions .....	2
3. Equipotential lines for two semi-infinite plates and electric field contour for a 1-V/m field between two plates .....	6
4. Normalized comparison of calculated and measured $E_z$ -field at location (0.1, 2, 0.025) .....	7
5. Normalized comparison of calculated and measured $H_z$ -field at location (0, 2, 0.69) .....	8
6. Normalized comparison of calculated and measured $E_z$ -field at location (-1, 2, 0.025) for live fire at 13 kV .....	9
7. Normalized comparison of calculated and measured $H_z$ -field at location (-1, 2, 0.89) for live fire at 13 kV .....	9
8. Normalized comparison of calculated and measured $E_x$ -field at location (-1, 2, 0.89) for live fire at 11 kV .....	10
9. Normalized comparison of calculated and measured $H_y$ -field at location (-1, 2, 0.076) .....	10
10. Normalized comparison of calculated and measured $E_z$ -field at location (-1, 2, 0.86) for live fire at 7 kV (3 plates) .....	11
11. Normalized comparison of calculated and measured $H_y$ -field at location (0, 2, 0.076) for live fire at 7 kV (3 plates) .....	11

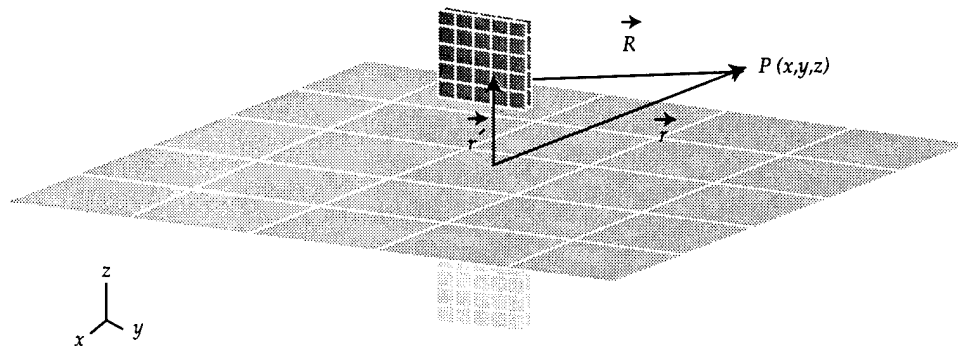
# 1. Introduction

Electromagnetic (EM) armor is a conceptual system that uses the formation of a current flow through a threat (once it is between a set of electrified plates) to interfere with armor penetration. Experiments were conducted previously on such a system for a "Walker plate" geometry [1] powered by a 6.6-mF capacitor bank with charging voltages up to 13 kV. These experiments allowed a limited number of electric ( $E$ -field) and magnetic ( $H$ -field) measurements to be made in the vicinity of the electrified plates under "calibration" (i.e., shorted) and "live-fire" conditions. For modeling purposes, we assumed that the experimental configuration was an alternating electric current filament centered between two plates that were located over a ground plane. Further, we assumed that the metal plates and ground plane were perfectly conducting. We referenced the field mapping to a rectangular coordinate system, and normalized data to the measured peak current amplitude and the current element length (i.e., the plate separation). We show the available data in comparison to the EM field of a transient electric current element oriented horizontally to a perfectly conducting plane. We estimated the influence of the conducting plates, and used an attenuation factor in the analytical results to allow meaningful comparisons.

## 2. Experiment

The field mapping coordinate system and the Walker plate geometry, imaged in the ground plane, is drawn to scale in figure 1. On this scale, the pair of plates looks like a single plate, since the plate area is much larger than the separation. The external circuit and supporting structure are not shown. The plates are mounted in a steel frame, which is bolted to a steel pad that is connected to an earth ground roughly 50 m away. The coordinate system origin is centered between the plates, but is located on the metal ground plane. The field point,  $P$ , is located by its  $(x,y,z)$  coordinates, in meters. The conducting plates are octagons roughly 0.76 m across, with a separation distance,  $l$ , of about 5 cm. The plates are 25-mm-thick aluminum, with removable 6-mm metal "break plates" in the center. The plates can be shorted by a calibration fixture consisting of a thin metal rod, or by

Figure 1. Field mapping coordinate system and Walker plate geometry imaged in a perfectly conducting ground plane.



a munition piercing the break plates. In either case, an intense current channel is formed with a damped sinusoidal waveform. The experiment is modeled as a current filament centered between the plates at a height  $h = 0.91$  m above the ground plane, with an image located at  $-0.91$  m below the ground plane.

The external circuit can be modeled as a series combination of resistance ( $R$ ), inductance ( $L$ ), and capacitance ( $C$ ), where the circuit parameters are estimated from the charging capacitance ( $C = 6.6$  mF) and the measured current waveform. The measured current implies an underdamped circuit with zero initial current, so the transient current can be approximated by

$$I(t) = I_0 e^{-\alpha t} \sin(\omega_d t) = I_0 e^{-\alpha t} \sin(2\pi f_d t), \quad (1)$$

where

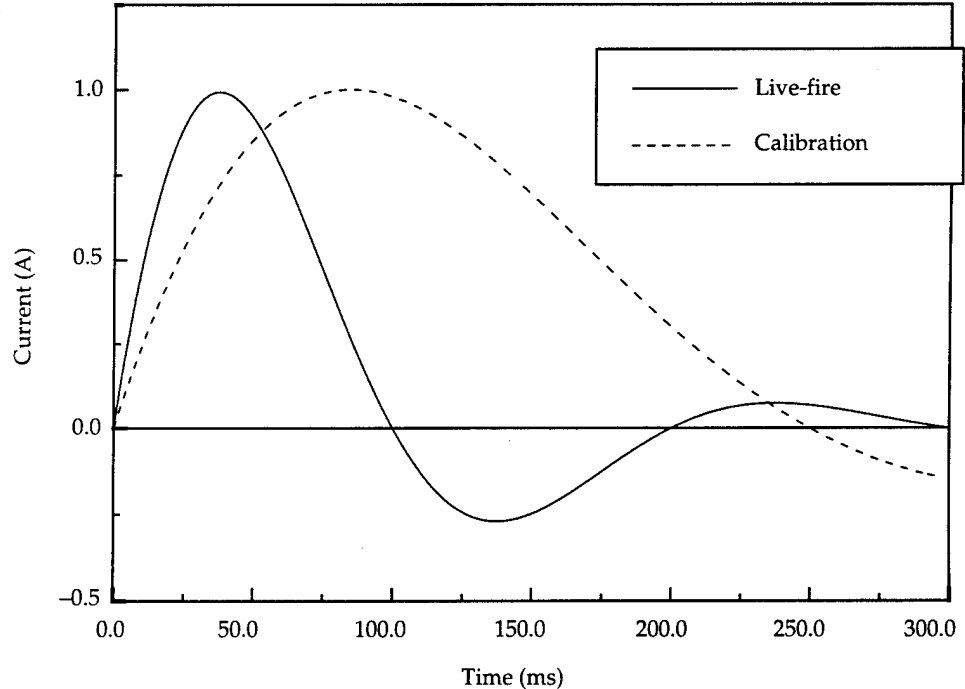
$$\omega_d = \sqrt{\omega_0^2 - \alpha^2}, \quad (2)$$

$$\alpha = \frac{R}{2L}, \text{ and} \quad (3)$$

$$\omega_0 = \frac{1}{\sqrt{LC}}, \quad (4)$$

with  $f_d$  the resonant frequency and  $\alpha$  the damping coefficient of the series-RLC circuit. These circuit parameters are not the same for the calibration fixture and live munitions. From the measured current waveform, we estimated that  $\alpha \approx 1.3 \times 10^4 \text{ s}^{-1}$  and  $f_d \approx 5 \text{ kHz}$  under live-fire conditions, as shown in figure 2 (with  $I_0 = 1.75 \text{ A}$  for unit peak amplitude), which implies that  $R \approx 3.4 \text{ m}\Omega$  and  $L \approx 0.13 \text{ }\mu\text{H}$ . For the calibration fixture, we estimated

Figure 2. Analytical fit to normalized input current for live-fire and calibration conditions.



that  $\alpha \approx 7000 \text{ s}^{-1}$  and  $f_d \approx 2 \text{ kHz}$ , as shown in figure 2 (with  $I_0 = 2.07 \text{ A}$  for unit peak amplitude), which leads to  $R \approx 10.8 \text{ m}\Omega$  and  $L \approx 0.77 \text{ }\mu\text{H}$ . Thus, the calibration fixture has added inductance and resistance to the system. The time to reach the peak current amplitude,  $I_p$ , is

$$t_p = \frac{\arctan \frac{\omega_d}{\alpha}}{\omega_d}, \quad (5)$$

which leads to  $t_p = 37.5 \text{ }\mu\text{s}$  under live-fire conditions, but  $t_p = 79.1 \text{ }\mu\text{s}$  for the calibration fixture, as shown in figure 2.

Selected vector components of the transient  $E$ -fields and  $H$ -fields are measured at various locations with respect to the coordinate system shown in figure 1, where we take our error in the sensor position as  $\pm 5 \text{ cm}$ . These field sensors have known transfer functions as described elsewhere [2]. The  $E$ -field is measured directly, but the time-derivative of the  $H$ -field is measured and numerically integrated [3]. The total measurement error includes the uncertainty in the field point location, and systematic errors (such as spurious noise sources) are conservatively estimated at  $\pm 14$  percent [4]. The EM field data are normalized to the peak source strength,  $p_p = I_p l$ , which is the measured peak current times the element length, where the transient source,  $p(t)$ , has the form of equation (1).

### 3. Analysis

The normalized measurements are shown in comparison to the EM field of a horizontal,  $x$ -directed alternating electric current element above a perfectly conducting plane [5]. In rectangular coordinates,  $\vec{r} = x \hat{x} + y \hat{y} + z \hat{z}$  locates the observation point ( $P$  in fig. 1), and  $\vec{r}' = x' \hat{x} + y' \hat{y} + z' \hat{z}$  locates the source current element centered between the plates. The origin of the coordinate system is located on the ground directly below the plate center so that  $x' = y' = 0$  and  $z' = \pm h$ . Then in our coordinate system,  $\vec{r}' = \pm h \hat{z}$  for the element and its image, respectively. The distance between the source and observation points is  $|\vec{R}| = |\vec{r} - \vec{r}'|$ , and we define  $Z = z \mp h$  for the current element and its image, respectively. We use a time-domain formulation for the EM field in free space of a transient current element as in equation (1). The current distribution is assumed to be uniform over the element length, since  $l \ll \lambda$ . The ground plane is accounted for by an image of the current element, with the total EM field in the upper half space obtained by superposition.

### 3.1 EM Field of an Alternating Electric Current Element

For our alternating electric current element,  $p(t)$ , located in free space, the transient EM field components are normalized to  $p_p$ . The EM field in rectangular coordinates is [6]

$$E_x(t) = \frac{\eta}{4\pi I_p R^2} \left[ \frac{x^2 - R^2}{Rc} \frac{\partial I(\tau)}{\partial t} + \frac{3x^2 - R^2}{R^2} \left( I(\tau) + \frac{c}{2R} \text{sgn}(t) \otimes I(\tau) \right) \right], \quad (6)$$

$$E_y(t) = \frac{\eta xy}{4\pi I_p R^2} \left[ \frac{1}{Rc} \frac{\partial I(\tau)}{\partial t} + \frac{3I(\tau)}{R^2} + \frac{3c}{2R^3} \text{sgn}(t) \otimes I(\tau) \right], \quad (7)$$

$$E_z(t) = \frac{\eta xZ}{4\pi I_p R^2} \left[ \frac{1}{Rc} \frac{\partial I(\tau)}{\partial t} + \frac{3}{R^2} I(\tau) + \frac{3c}{2R^3} \text{sgn}(t) \otimes I(\tau) \right], \quad (8)$$

$$H_y(t) = \frac{-Z}{4\pi I_p R} \left[ \frac{1}{Rc} \frac{\partial I(\tau)}{\partial t} + \frac{I(\tau)}{R^2} \right], \text{ and} \quad (9)$$

$$H_z(t) = \frac{y}{4\pi I_p R} \left[ \frac{1}{Rc} \frac{\partial I(\tau)}{\partial t} + \frac{I(\tau)}{R^2} \right], \quad (10)$$

where  $\eta = 120\pi\Omega$  is the free-space impedance,  $t$  is the time,  $c$  is the speed of light,  $\tau = t - R/c$  is the retarded time,  $\text{sgn}(t) = t/|t|$  for  $t \neq 0$ , and  $\otimes$  is the convolution operator. These equations hold for all field points and all times, although the radiation terms are negligible at the field points of interest. Similarly, the retarded time is retained for completeness, although  $\tau \approx t$  for the field points of interest. The presence of the ground plane is accounted for by an appropriate image element located in the lower half space for which  $Z = z + h$ . Then equations (6) to (10) are used to calculate the field components for the image element in the upper half-space where the total EM field at the observation point,  $P$ , is the superposition of the EM field, owing to the source and image current elements.

In this formulation, physical considerations must be used when calculating the transient  $E$ -field for a current waveform that has a nonzero dc value. The convolution term in equations (6) through (8) can be written as

$$\text{sgn}(t) \otimes I(t - R/c) = - \int_{t-R/c}^{\infty} I(t') dt' + \int_0^{t-R/c} I(t') dt' = 2 \int_0^{t-R/c} I(t') dt' - \int_0^{\infty} I(t') dt', \quad (11)$$

where  $t' = t - (R/c) - s$  and  $dt' = -ds'$ . The last integral in equation (11) represents the dc value of the source current  $I(t)$ , and serves as a constant of integration. The numerical implementation of this approach has been validated against the Numerical Electromagnetics Code version 4.1 (NEC4) [7], where the NEC4 result in the time domain is obtained by Fourier inversion.

In our analysis,  $I(t)$  as in equation (1) has a dc component, but the initial current is zero, so the contribution of this dc component is neglected in the field calculations in order to provide physical results. The NEC4 frequency domain formulation (i.e.,  $l \ll \lambda$ ) can also lead to nonphysical transient results for an arbitrary source current, depending on the Fourier transform techniques used. Calculating the EM field directly in the time domain was found to be more practical; however, a dc component of the source current leads to static fields, which must be ignored. We estimate the influence of the plates in the next section, based on an electrostatic model of the electrified plates in two dimensions.

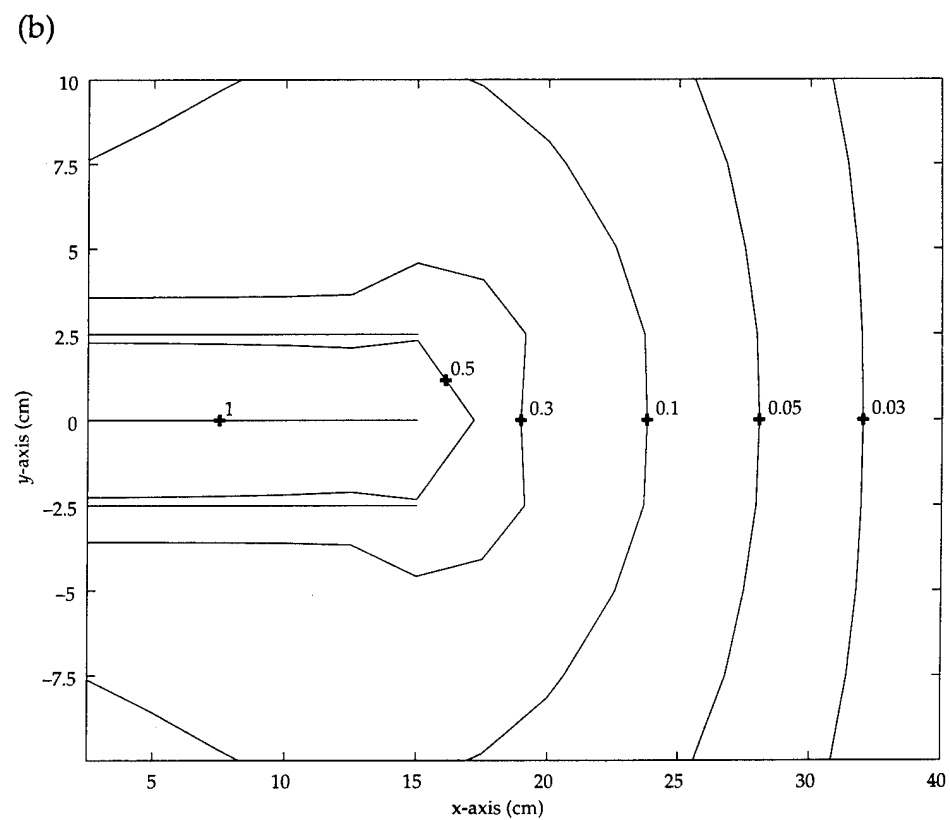
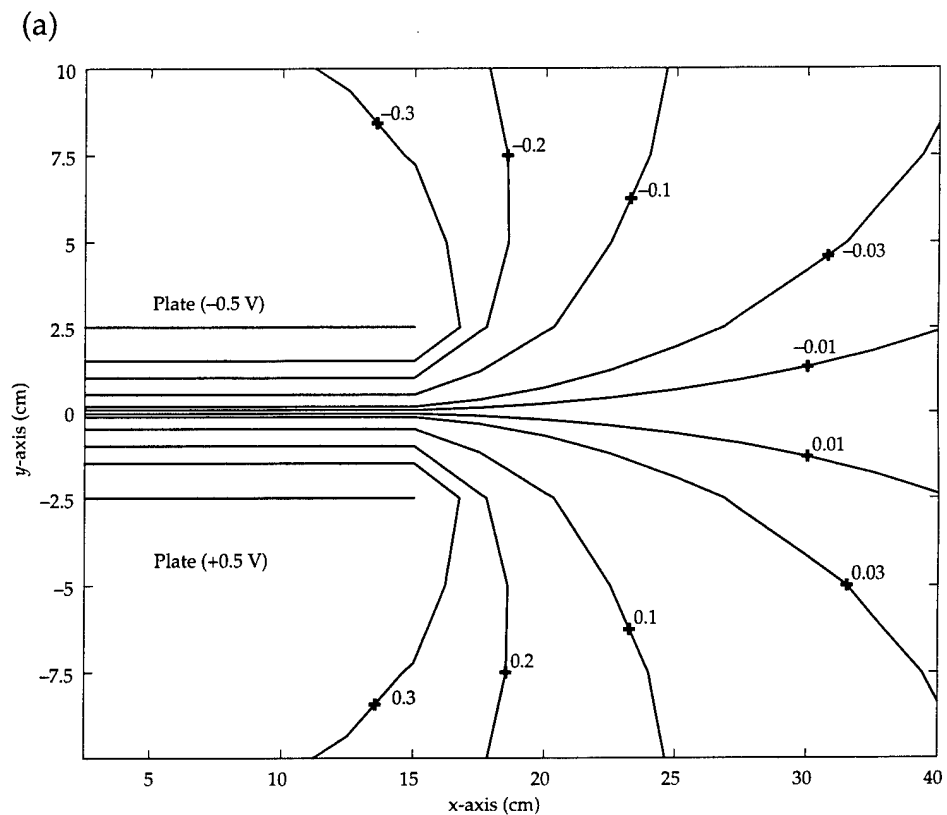
### 3.2 Electrostatic Field of Semi-Infinite Plates

The calculated EM field of the current element does not account for the fringing field effect owing to the presence of the conducting plates. A complete model of the electrified plate system was beyond the scope of this preliminary effort, so the fringing field effect was estimated separately. This effect is treated as an attenuation parameter that is estimated from a solution for the electrostatic field outside the plates, which are assumed of infinite vertical extent (i.e., along the  $z$ -axis). This numerical solution involves an array of 61 charged strips across the plates for which the Poisson equation can be solved analytically. Since the field points of interest are nearly perpendicular to the  $z$ -axis, the fact that the plates are infinite in this transverse direction is not a severe limitation on the application of this model to the experimental configuration.

The equipotential lines near the plates are shown in figure 3(a), where the plates are held at a potential of  $\pm 0.5$  V, which leads to a zero equipotential line centered between the plates. Figure 3(a) is consistent with the classical result for the equipotential lines of a parallel-plate capacitor [8]. The corresponding  $E$ -field lines (i.e., the vector magnitude of the  $E$ -field) near the plates are shown in figure 3(b). For normalized results, the charge on the plates is adjusted to result in a uniform  $E$ -field of 1 V/m between the plates. At ranges more than about three plate diameters, the fringing field decays inversely as the distance is cubed, as in an array of electrostatic dipoles. Note that the  $E$ -field at points perpendicular to the plates (i.e., the  $x$ -axis) would be small compared to the field off the end of the plates (i.e., the  $y$ -axis). For field points near the plates, the attenuation factor can be estimated from figure 3(b); however, at larger distances, this factor is simply a  $1/R^3$  decay. We apply this type of electrostatic attenuation factor to the alternating current element between conducting plates as a crude, but realistic, way to estimate the influence of the plates on the EM field.

If we take a reference point within the plates where the field is nearly uniform, we can estimate the fringing field distribution at larger distances. Consider a reference point near the center of the plates (e.g., at  $R_0 = 2.5$  cm). For our field points at  $R = 2.2$  m, we have  $(R_0/R)^3 = 1.4 \times 10^{-6}$ . This attenuation factor is used for the  $E$ -field, but it does not directly apply to the  $H$ -field. As a first approximation, we assume that the conducting plates influence the  $H$ -field in the same manner, according to Maxwell's equations.

Figure 3.  
 (a) Equipotential lines for two semi-infinite plates and  
 (b) electric field contour for a 1-V/m field between two plates.



For an electric current element, the wave impedance at the field point locations is about  $1.2 \times 10^4 \Omega$ , so we use an  $H$ -field attenuation factor of  $1.7 \times 10^{-2}$ . The same attenuation factor is applied to the EM field of the current element image, since it is also centered between conducting plates. Thus, the total  $E$ -field calculated in the upper half space is reduced by 123 dB, and the total  $H$ -field is reduced by 35 dB for comparison to the measured data.

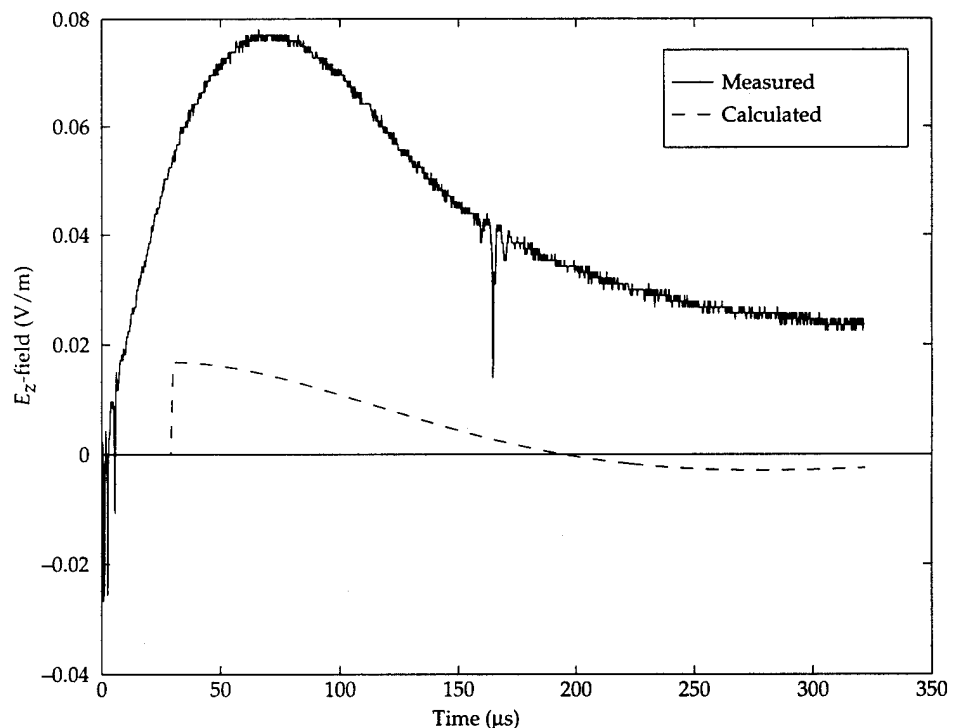
## 4. Results

We locate the observation points (and vector components) of the measured EM field in a rectangular coordinate system (see fig. 1), so the results are referenced to the  $(x,y,z)$  coordinates in meters. Since the plate voltage polarity is arbitrary, the calculated and measured results are all shown with a positive polarity for clarity. Under calibration conditions, the plates are shorted with a metal rod and discharged by a spark gap switch. When shorted, the circuit has a somewhat different impedance and, therefore, a different current waveform compared to live munitions.

### 4.1 EM Field Measurements for a Calibration Configuration

The normalized comparison for the  $z$ -component of the  $E$ -field at location  $(0.1, 2, 0.025)$  is shown in figure 4 for the calibration fixture configuration. For  $x = 0$ , the calculated  $E$ -field component at this location would be zero, so we moved the measurement location to be within 0.1 m of  $x = 0$ . Note the initial burst of switching noise and evidence of arcing at  $160 \mu\text{s}$ , which is typical of all the measured  $E$ -field data. The agreement between the

Figure 4. Normalized comparison of calculated and measured  $E_z$ -field at location  $(0.1, 2, 0.025)$ .



measured and calculated result is not very good. The large discrepancy in amplitude could be due to the  $E$ -field of the spark gap switch (and external circuit), which is neglected in the calculated field. The normalized comparison results for the  $z$ -component of the  $H$ -field at location  $(0, 2, 0.69)$  are shown in figure 5 for the same plate configuration. The agreement between the measured and calculated results is not very good. The discrepancy in amplitude could be associated with the calibration fixture, because the  $H$ -field contribution from the large current in the wire connections to the plates is probably not negligible.

## 4.2 EM Field Measurements for a Live Munition Configuration

For live munitions, the normalized comparisons between the measured and calculated results are shown in figures 6 to 11. The charging voltage is either 11 or 13 kV in the two-plate configuration or, for a three-plate configuration, the charging voltage is 7 kV across each set of plates. A comparison for the  $z$ -component of the  $E$ -field at location  $(-1, 2, 0.025)$  is shown in figure 6 for a 13-kV voltage across the plates. In this case, the agreement between the measured and calculated results is very good. The noise in the first 25  $\mu\text{s}$  (which is clipped) is associated with the  $E$ -field from flash x-ray equipment. The repetitive noise signals, which appear during the  $E$ -field risetime and have a period of roughly 25  $\mu\text{s}$ , are probably reflections of early-time arcing transients, where the period depends on the experiment grounding configuration.

Figure 5. Normalized comparison of calculated and measured  $H_z$ -field at location  $(0, 2, 0.69)$ .

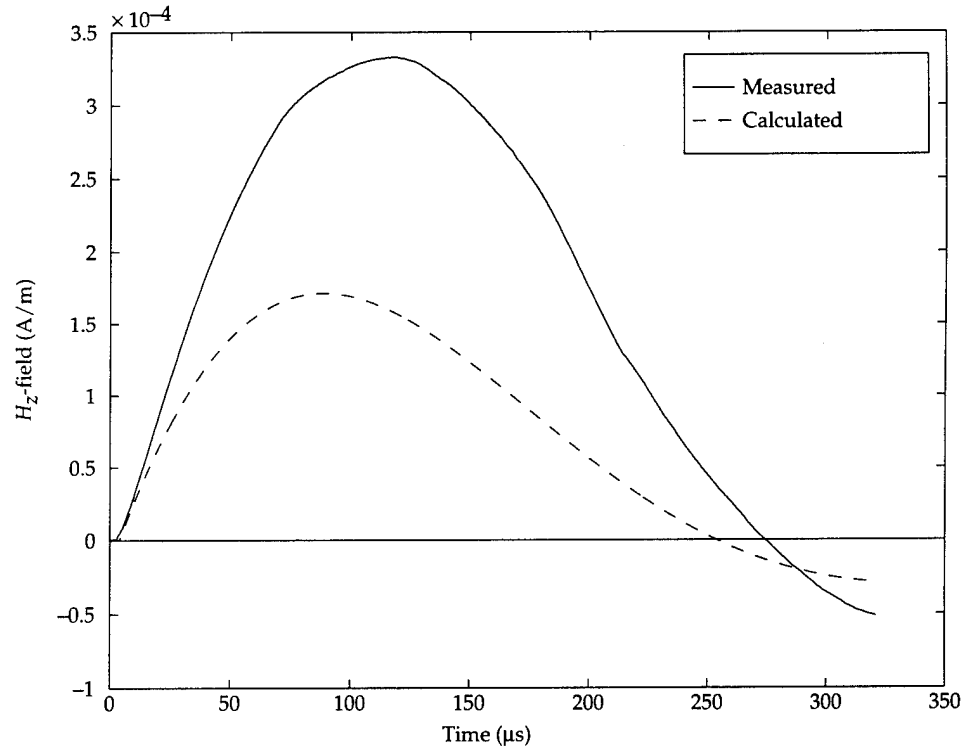


Figure 6. Normalized comparison of calculated and measured  $E_z$ -field at location  $(-1, 2, 0.025)$  for live fire at 13 kV.

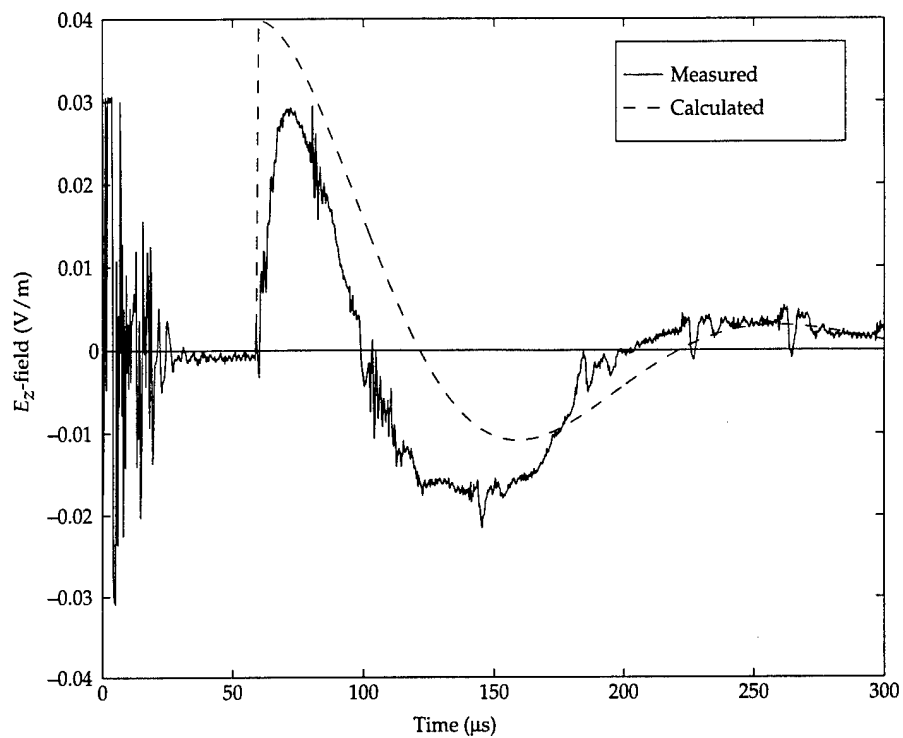
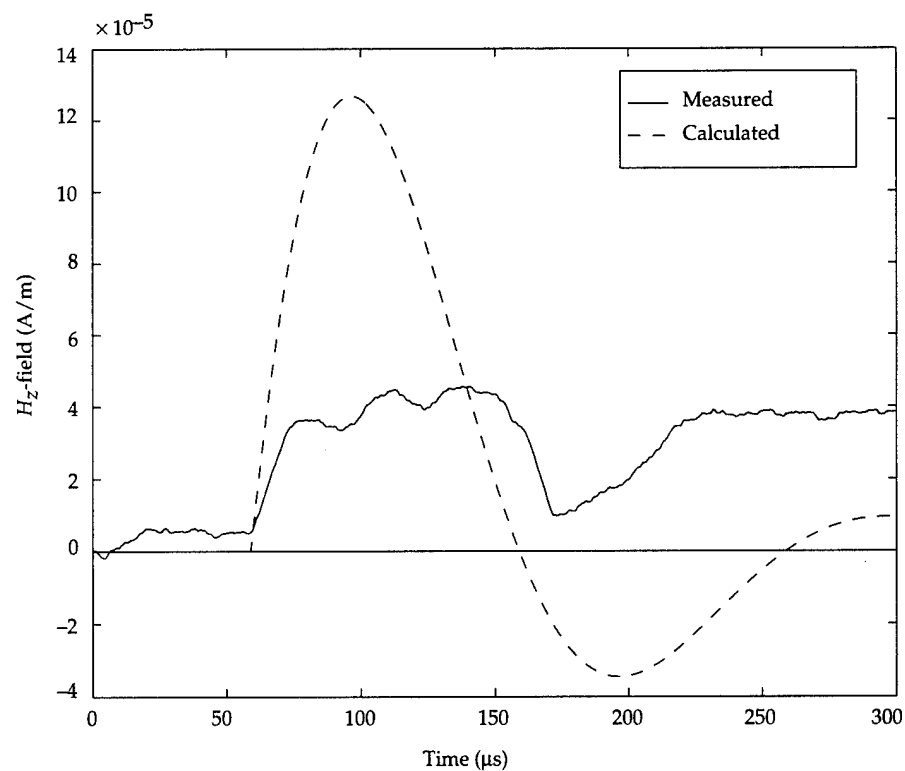
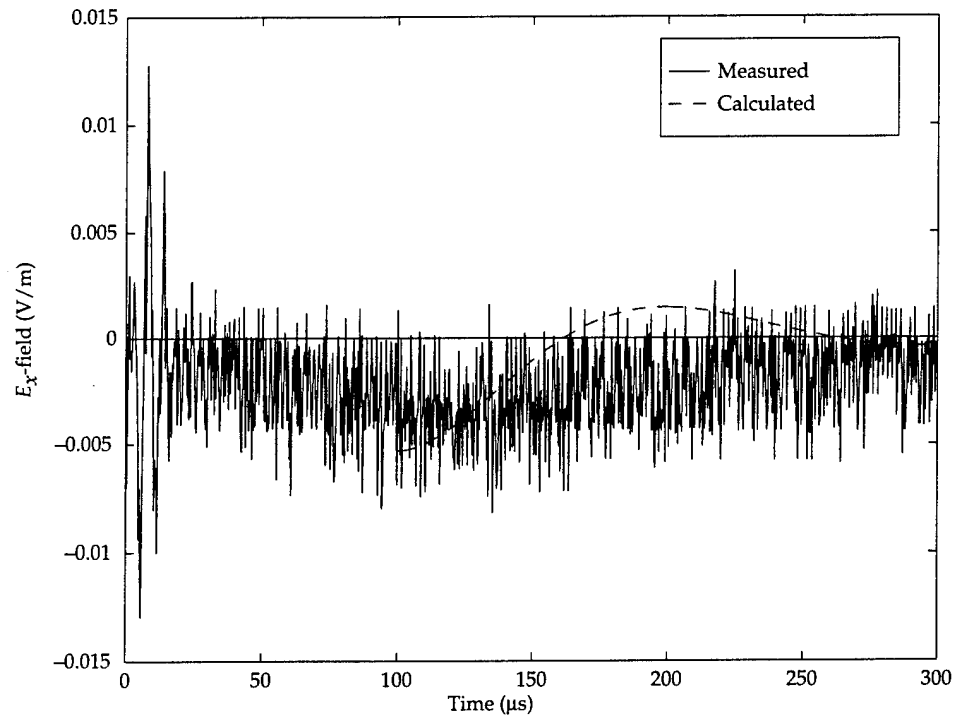


Figure 7. Normalized comparison of calculated and measured  $H_z$ -field at location  $(-1, 2, 0.89)$  for live fire at 13 kV.



**Figure 8. Normalized comparison of calculated and measured  $E_x$ -field at location  $(-1, 2, 0.89)$  for live fire at 11 kV.**



**Figure 9. Normalized comparison of calculated and measured  $H_y$ -field at location  $(-1, 2, 0.076)$ .**

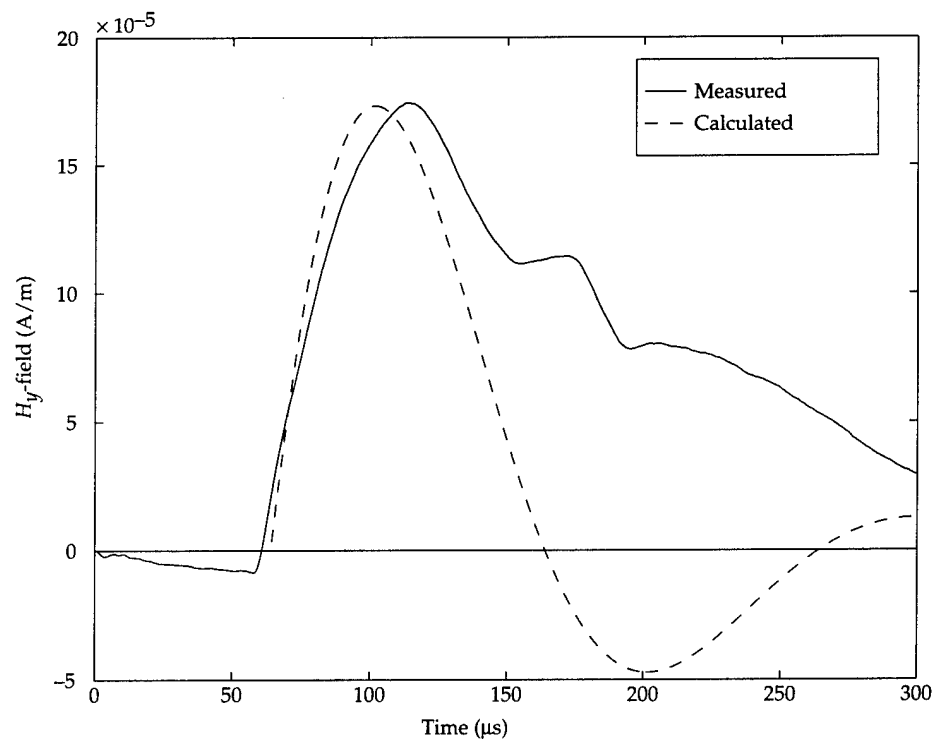


Figure 10. Normalized comparison of calculated and measured  $E_z$ -field at location  $(-1, 2, 0.86)$  for live fire at 7 kV (3 plates).

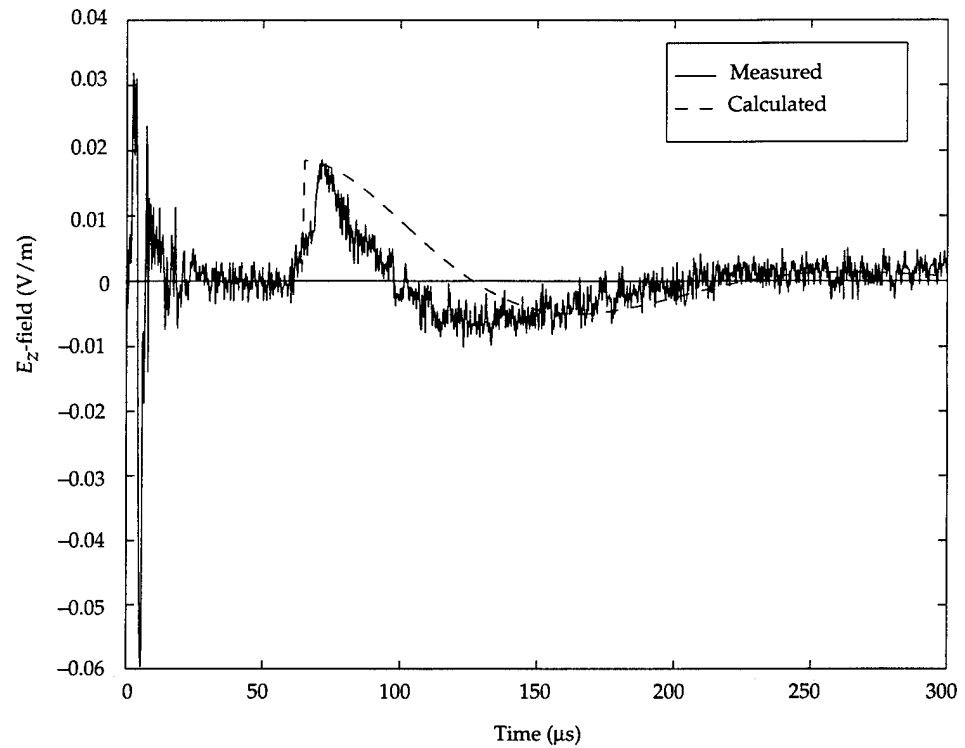
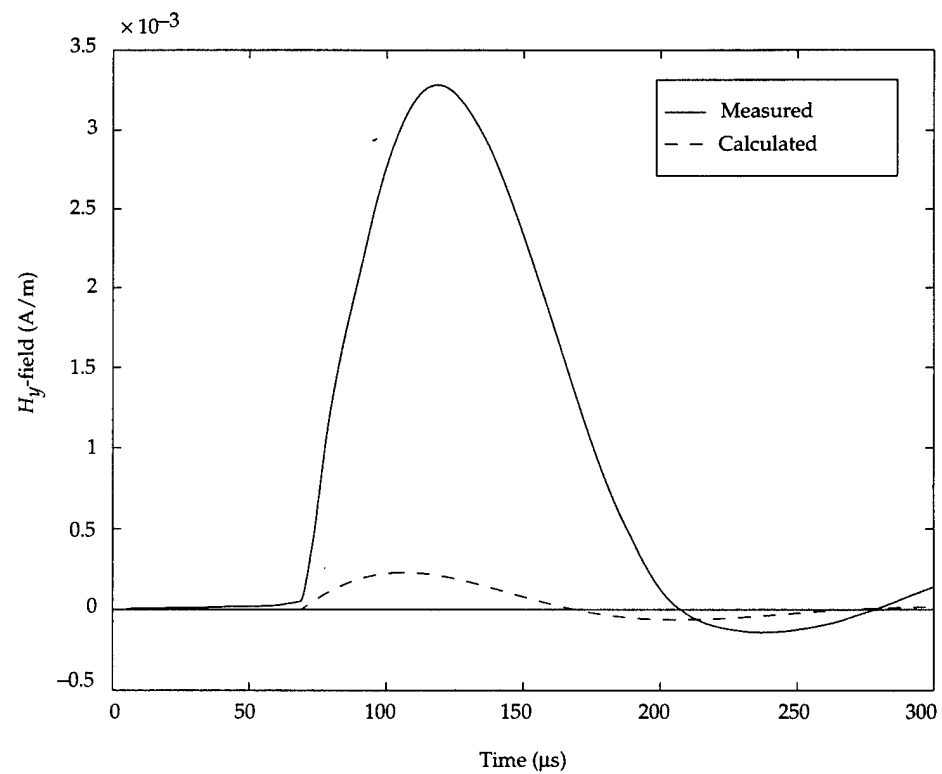


Figure 11. Normalized comparison of calculated and measured  $H_y$ -field at location  $(0, 2, 0.076)$  for live fire at 7 kV (3 plates).



The normalized comparison for the  $z$ -component of the  $H$ -field at location  $(-1, 2, 0.89)$  is shown in figure 7 for a charging voltage of 13 kV. In the measured data, a late-time source current is evident. For this reason, comparisons between the measured and calculated  $H$ -field are, typically, not as good as those for the  $E$ -field. The  $H$ -field data imply a current flowing after the discharge event, but no substantial late-time (i.e.,  $>200 \mu\text{s}$ )  $E$ -field is measured. Although it is not clear why the late-time  $E$ -field and  $H$ -fields are so different, the implication is a late-time  $H$ -field source, such as current flowing in a loop. Note that the repetitive noise signals that appear in the  $E$ -field data every  $25 \mu\text{s}$  (see fig. 6) are also evident in the  $H$ -field data (see fig. 7). However, the measured  $H$ -field does not indicate a significant noise contribution from the flash x-ray equipment, as could be expected for such a high-voltage source. The late-time peak in the transient  $H$ -field is not consistent with reflections from nearby metal objects or the grounding scheme at the experimental range, so we associate this late-time signal with loop currents flowing in the support structure and metal pad.

For a charging voltage of 11 kV, the normalized comparison for the  $x$ -component of the  $E$ -field at location  $(-1, 2, 0.89)$  is shown in figure 8. This is one example of several null measurements that were designed to identify the negligible EM field components. Even though the measured data are almost obscured by noise, the comparison implies consistency with the calculated result. For an  $x$ -directed current element over a perfect ground, this  $E$ -field component would be small or zero (depending on the exact field-point location), so the data are consistent with the radiation pattern of an oscillating current element over a conducting ground plane.

The normalized comparison for the dominant component of the  $H$ -field at location  $(-1, 2, 0.076)$  is shown in figure 9 where, again, a low-frequency  $H$ -field is evident. The agreement between the measured and calculated results in early time is very good. The measured  $H$ -field more closely follows the  $E$ -field, but indicates an additional source current at late times. Null measurements for the  $x$ -component of the  $H$ -field (not shown), and the reasonable agreement for the dominant components of the EM field, support the conclusion that an EM armor system would have a radiation pattern similar to that of an electric current element located over ground.

In the three-plate configuration, a 7-kV voltage is used between the center plate and the front and rear plates. For convenience, this experimental configuration is modeled in the same manner, rather than as two separate source current elements. The normalized comparison result for this configuration is shown in figure 10 for the  $z$ -component of the  $E$ -field at location  $(-1, 2, 0.86)$ , and the agreement is very good. For the  $y$ -component of the  $H$ -field at location  $(0, 2, 0.076)$ , the normalized comparison is shown in figure 11. Note that the measured  $H$ -field follows the transient current in this configuration, which implies that the source current initiated between the plates does not continue for late times. However, there is a large discrepancy in the measured and calculated amplitudes. Based on the calculated  $H$ -field, a single current element is not a good model for this plate configuration. The data indicate that the three-plate configuration produces an order-of-magnitude larger  $H$ -field than might be expected for the two-plate configuration.

## 5. Conclusion

The transient EM environment of an electrified plate system is similar to that of an alternating electric current element, but complicated by the influence of the conducting plates, the external circuit, and the experimental configuration. An isolated element over a perfect ground plane provides some insight into the nature of the measured EM environment, but requires an estimated attenuation parameter to account for the influence of the plates. A more realistic model for a current channel between conducting plates should be used in the future. The effects of the external circuit and nearby metal structures should also be included in a complete model of a Walker plate system, since the metal support structure and grounding configuration can significantly influence the EM environment. The measured data indicate that the EM field associated with an EM armor system would be a source of interference on the modern battlefield. An understanding of this EM environment is a prerequisite for using such an advanced armor system on military platforms.

In this preliminary study, a simple theory was desired that could be used to estimate the temporal and spatial variations of the EM environment. An alternating electric current element over a perfect ground plane has proven to be useful for this purpose. Although an undesirable estimated parameter is required for comparison to the measured data, the approximate theory allows engineering predictions for the EM environment associated with this experiment. The limited amount of measured data indicates that the radiation pattern would be similar to that of a horizontal current element over a ground plane. The null in this pattern is in the direction of the current element, which also corresponds to the minimum field outside the plates. Thus, the EM environment would be small in the current direction (i.e., the projectile flight path) and much larger in the transverse direction. More detailed EM models and additional EM field data are planned for future electrified plate experiments. Further experimental and theoretical investigations of the EM environment are required to address EM compatibility and battlefield signature issues for this type of conceptual armor system.

## Acknowledgments

The authors would like to thank the many other personnel of WT-WD and WT-TA who conducted these experiments for allowing us to participate. In particular, we would like to acknowledge Dick Carroll, Tom Barnhill, Kevin Binkley, Gregory Gentle, and the rest of the staff at Range 7. Without their help, these EM field measurements would not have been possible. Additionally, we would like to thank Chuck Hummer, Clint Hollandsworth, and Paul Berning for their comprehensive technical review and many helpful suggestions.

## References

1. E. H. Walker, *Defeat of Shaped Charge Devices by Active Armor*, U.S. Army Ballistic Research Laboratory, BRL-MR-2309 (July 1973).
2. W. O. Coburn, C. Le, and H. Martin, *EM Field Measurements Near a Single-Stage Reconnection Gun*, U.S. Army Research Laboratory, ARL-MR-206 (April 1995).
3. W. O. Coburn, C. Le, D. DeTroye, G. Blair, and W. Williams, *EM Field Measurements Near a Rail Gun*, IEEE Trans. Magn. **31**, No. 1 (January 1995), pp 692–697.
4. W. O. Coburn and C. Reiff, *Wideband Pulse Attenuation of an Uncured Metalized Glass Fiber Mat*, U.S. Army Research Laboratory, ARL-TR-790 (September 1995).
5. T. S. M. Maclean and Z. Wu, *Radiowave Propagation Overground*, Chapman and Hall (1993).
6. B. Luu and C. Le, *AESOP Field Prediction*, U.S. Army Research Laboratory, ARL-TR-835 (October 1995).
7. G. J. Burke, *Numerical Electromagnetics Code—NEC—4 Method of Moments (NEC—4.1)*, Lawrence Livermore National Laboratory, UCRL-MA-109338 (January 1992).
8. P. M. Morse and H. Feshbach, *Methods of Theoretical Physics*, McGraw-Hill (1953), p. 1245.

## Distribution

Admnstr  
Defns Techl Info Ctr  
Attn DTIC-DDA  
8725 John J Kingman Rd Ste 0944  
FT Belvoir VA 22060-6218

Dir  
Defns Intllgnc Agcy  
Attn RTS-2A Techl Lib  
Washington DC 20301

Defns Nuc Agcy  
Attn RAES Elect Syst Techlgy Div  
Attn RAST Electromagnetic Applctn Div  
Attn TITL Tech Lib  
6801 Telegraph Rd  
Alexandria VA 22310-3398

Defns Nuc Agency Office of Techl  
Applications  
Attn D R Lewis  
6801 Telegraph Rd  
Alexandria VA 22310

Ofc of the Assist Secy of the Army for Rsrch  
Dev & Acqstn  
Attn SARD-TR Dr R Chait  
Room 3E476 The Pentagon  
Washington DC 20310-0103

Cmdr  
US Army ARDEC  
Attn AMSTA-AR-AEC-IE N Svendsen  
Attn AMSTA-AR-CCL-D W Williams  
Bldg 65 N  
Picatinny Arsenal NJ 07806-5000

US Army AVRDEC  
Attn AMSAT-R-EFM P Haselbauer  
4300 Goodfellow Blvd  
ST Louis MO 63120-1798

US Army BRDEC  
Attn SATB-FGE J Ferrick  
Attn SATB-FGE T Childers  
FT Belvoir VA 22060-5606

US Army Matl Cmnd  
Attn AMCAM-CN  
5001 Eisenhower Ave  
Alexandria VA 22333-0001

Dir  
US Army Mis Cmnd (USAMICOM)  
Attn AMSMI-RD-CS-R Documents  
Redstone Arsenal AL 35898-5400

Cmdr  
US Army MRDEC  
Attn AMSMI-RD-ST-CM J Vandier  
Huntsville AL 35898-5240

US Army Natick RDEC  
Attn SATNC-SUSD-SHD A Murphy  
Kansas Stret  
Natick MA 01760-5018

US Army Nuc & Chem Agcy  
Attn MONA-NU R Pfeffer  
7150 Heller Loop Rd Ste 101  
Springfield VA 22150

US Army TARDEC  
Attn AMSTA-ZT G Baker  
Warren MI 48397-5000

US Army TECOM  
Attn STERT-TE-E J Knaur  
Redstone Technical Test Center  
Huntsville AL 35898-8052

US Army TECOM Techl Dir Ofc  
Attn AMSTE-TC-D R Bell  
Aberdeen Proving Ground MD 21005

Nav Rsrch Lab  
Attn Code 4820 Techl Info Div  
4555 Overlook Ave SW  
Washington DC 20375-5000

Cmdr  
Nav Surfc Weapons Ctr  
Attn Code E231 Techl Lib  
Dahlgren VA 22448-5020

## Distribution

Nav Warfare Ctr  
Attn Code OZT T Conway  
Lakehurst NJ 08733

Dir Air Force Armament Directorate  
Attn WL/MNAA S Federle  
101 W Eglin Blvd. Ste 346A  
Eglin AFB FL 32542-6810

Natl Inst of Stand & Techlgy  
Attn V Ulbrecht Rsrch Info Ctr  
Rm E01 Bldg 101  
Gaithersburg MD 20899

DoD Joint Spectrum Ctr  
Attn CA J Word  
120 Worthing Basin  
Annapolis MD 21401

US Army Rsrch Lab  
Attn AMSRL-WT-PB Chf  
Attn AMSRL-WT-WD A Prakash  
Attn AMSRL-WT-WB Chf  
Attn AMSRL-WT-WC Chf  
Attn AMSRL-WT-WD Chf  
Rm 243A Bldg 120  
Aberdeen Proving Ground MD 21005

US Army Rsrch Lab  
ARDEC  
Attn AMSTA-AR-AEF-A Chf  
Adelphi MD 20783-1197

US Army Rsrch Lab  
Attn AMSRL-OP-SD-TA Mail & Records  
Mgmt  
Attn AMSRL-OP-SD-TL Tech Library  
(3 copies)  
Attn AMSRL-OP-SD-TP Tech Pub (5 copies)  
Attn AMSRL-SE Chf  
Attn AMSRL-WT-N Chf  
Attn AMSRL-WT-NB Chf  
Attn AMSRL-WT-ND C Le  
Attn AMSRL-WT-ND Chf  
Attn AMSRL-WT-ND W O Coburn  
(5 copies)  
Attn AMSRL-WT-NE Chf  
Attn AMSRL-WT-NF Chf  
Attn AMSRL-WT-NG Chf  
Attn AMSRL-WT-NH Chf  
Attn AMSRL-WT-NJ Chf  
Attn AMSRL-WT-N Sr Rsrch Scntst  
Attn AMSRL-WT-ND J Latess  
Adelphi MD 20783-1197